Synthesis And AB Initio Structure Determination Of Transition Metal Mixed Valence Oxide $Cu_{0.45} Mo_{1.25} O_9 V_{2.23}$ By Powder XRD And Study The Physical Property

Bimal K. Kanth and Parashuram Mishra*,

Bioinorgani and Materials Chemistry Research Lab.M.M.A.M.Campus,Tribhuvan University,Biratnagar,Nepal

Abstract: This paper is intended the ab initio structure determination of the transition metal framework mixed valence $Cu_{0.45} Mo_{1.25} O_9 V_{2.23}$ from precession electron diffraction intensities AND POWDER XRD. The metal framework of the compound was solved in this investigation via direct methods from Powder XRD.A subsequent (kinematical) least-squares refinement with electron intensities yielded slightly improved co-ordinates for the ternary metal oxide atoms in the structure. Chemical analysis of several crystallites by EDX is in agreement with the formula $Cu_{0.45} Mo_{1.25} O_9 V_{2.23}$ Moreover, the structure was independently determined by Rietveld refinement from X-ray powder data obtained from a multi-phasic sample. The compound having triclinic crystal system space group P-1 and centrosymmetry structure with refined lattice parameters a=4.8262 Å,b=6.3208 Å,c=10.4473 Å, α=88.4808° β=85.0982° γ=85.0740° and volume=316.30A³Comparison of the framework structure from electron diffraction with the result from Rietveld refinement shows an average agreement for the heavy atoms within 0.09A °. The titled compound was prepared from mixture of $CuCO_3$- MoO- VO5 by solid state reaction with full thermal decomposition at 1000°C. Rwp = 0.0680, Rp = 0.030 and GOF=0.31 and the structure factors F0 = 3023 and Fc = 3021.

-- ---------

Date of Submission: 06-07-2020   Date of Acceptance: 21-07-2020

-- ---------

I. INTRODUCTION

The fields of solid-state chemistry and materials science are searching for and discovering new functional materials. Recently, the theoretical prediction and experimental realization of thermodynamically stable materials have seen much research[1–4] and some success. Translating this progress to metastable materials systems, such as thermochemically unstable compounds produced by non-equilibrium thin film synthesis techniques, is an emerging frontier. For this vast metastable materials space, productive scientific approaches are lacking, because both theory and experiment face challenges here. Theoretical structure search methods are most mature when targeting ground state structures using energy as the search metric. Similarly, problematic, metastable materials are likely to be initially observed in small, strained crystals that present challenges for experimental structure determination methods, such as diffraction. The opportunity, on the other hand, is huge: for every ground-state structure, there are many hundreds of higher-energy structures that may be metastable. Also, these higher-energy polymorphs may have useful practical applications, such as (anti)ferroelectric materials[7,8].

In materials chemistry, the crystal structure determination is the first step to understand and interpret physical properties of an unknown material. Moreover, it also guides people on how to modify the material and hence improve the performance. Nowadays, the most successful technique for structure determination is through powder X-ray diffraction, from which a sufficient number of independent reflections against the structural parameters can be extracted in 3D reciprocal space[9]. Several mature analysis methods, such as the direct method, Patterson method, charge-flipping algorithm, and maximum entropy method can be applied to accurately solve the structure. This technique requires synthesizing a high quality powder at a micrometre level, which might be difficult in some fields, for example in ceramic chemistry [5]. In this case, powder X-ray diffraction (PXRD) becomes a popular technique[10]. The difficulty could further increase when the target phase is not the highly dominant one in the composition. To determine the structure of an unknown phase in a multi-phase polycrystalline sample would be very helpful for the researchers, saving time to optimize the syntheses conditions. Our understanding of the properties of materials is almost always based on structural information on the atomic scale. Such information is commonly obtained by the wide spread method of X-ray crystallography. However, due to the relatively weak interaction of matter with X-rays, this method is sufficient to investigate extremely small volumes or individual crystals at the scale[11]. Materials with pronounced twinning or new compounds that only exist as part of a complex multi-phase powder sample are thus extremely difficult to treat with this standard method for structure determination [12]. It should be noted that these problem

cases also include many technologically relevant products such as small precipitates in a metallic matrix, catalysts, pharmaceuticals, pigments and thin films, which a priori exist only in small quantities or rarely grow as large crystals. Hence, ample motivation exists to develop alternative approaches capable for structural analysis of extremely small volumes and crystallites. However, the only real alternative to X-rays is fast electrons, since their interaction with matter is several orders of magnitude stronger than that of X-rays. Electron diffraction structure analysis (EDSA) makes it, thus, possible to obtain structural information at the atomic level even for the steadily growing number of nanocrystalline materials[13]. On the other hand, structure analysis with electron data is rarely straightforward and fully automated, as it is the case with X-ray data because now-a-days powder X- ray diffraction has been routinely used a non-destructive fingerprinting technique. It has also been used in studies related to structural phase transitions at variable temperature and pressure. The aim of this work is determine structure of titled compound by ab initio method with the help of powder XRD and study the physical properties[14].

II. MATERIAL AND METHOD

All chemicals used were analytical grade. A polycrystalline sample of $Cu_{0.45}$ $Mo_{1.25}$ O_9 $V_{2.23}$. was synthesized by a standard solid state reaction using a mixture of high purity reagents of $CuCO_3$-MoO- V2O5 contained mixed valence as the starting materials in the molar ratio of 1 : 1 : 1. The mixture was ground carefully, homogenized thoroughly with methanol (99%) in an agate mortar followed stoicheiometrc and then packed into an alumina crucible and calcined at 1000°C in air for 30h with several intermediate grindings. Finally the product was pressed into pallets and sintered at 100 K/h. Powder X-ray diffraction (XRD) data were collected at room temperature in the angular range of 2q =10 to 90 with scan step width of 0.02° and a fixed containing time of 15 s using Philips powder diffractometer with graphite monochromatic CuKa radiation. The powder was rotated during the data collection to minimize preferred Orientation effect if any. The program TREOR in CRYSFIRE was used to index the powder pattern which give triclinic cell system.SIRPOW92 was used to locate the positional parameters of constituent atoms. The full pattern is fitting and peak decomposition in the space group P-1 using check cell program. The structural parameters were refined by the Reitveld method using the Jana program which gave at 1000°C. Rwp = 0.0680, Rp = 0.030 and GOF=0.31 the structure factors F0 = 3023 and Fc = 3021. The density is determined by Archimedes principle.The visual structure was determined by Diamond and Ortep program.

III. RESULTS AND DISCUSSIONS

In order to find out the size and to study the structural properties of the synthesized $Cu_{0.45}$ $Mo_{1.25}$ O_9 $V_{2.23}$ transiotion metal mixed valence by powder XRD analysis was performed. Structural identification of $Cu_{0.45}$ $Mo_{1.25}$ O_9 $V_{2.23}$ were carried out with X-ray diffraction in the range of angle 2θ between 20º to 70º. Figure.1 shows the XRD patterns for $Cu_{0.45}$ $Mo_{1.25}$ O_9 $V_{2.23}$ which were nanocrystalline in nature. It is clearly revealed that all of the peaks match well with the P-1 space group. Hence, all the reflected peaks in this pattern were found to match with the metal of mixed oxide phase having primitive triclinic crystal system. The broadened peak shows the nanometer-sized crystallites. The average crystalline size was calculated using the Debye-Scherrer formula,with FWHM and found 70.32 nm[15].

STRUCTURE SOLUTION
Reitveld Refinement

The framework structure of $Cu_{0.45}$ $Mo_{1.25}$ O_9 $V_{2.23}$ was first examined by ab initio structure determination method using the powder XRD data. The initial lattice parameters were determined to be parameters a=18.5243 Å, b=5.5290 Å, c=3.3335 Å, α=90.1230° β=90.5674° γ=90.6570° and V=341.38 $Å^3$. by an indexing procedure using the program TREOR15 in EXPO2004.16 The most probable space group was suggested to be P1 triclinic crystal system Next, the integrated intensities were extracted by the Le Bail method using the program Jana2006.14 A profile function and background function of the Le Bail method used in the present study were Pseudo-Voigt function and 20thorder Legendre function, respectively. An initial structure model was then obtained by the charge flipping (CF) method17 using the extracted integrated intensities. Although the Mo site could not be clearly determined by the CF

The iteration converged with an R factor of 29% and the final electron density shows a P1 symmetry with a 5% error. The program of EDMA was then used to automatically assign atomic positions. Four unique heavy atomic positions were found and the heaviest one was assigned as Bi while the others were considered as V and Mo. Due to the existence of heavy atoms, all oxygen positions were ambiguous in the electron density map of this stage[14]. To locate the oxygen atoms, a Monte-Carlo based simulated annealing process with the program TOPAS was applied. For each annealing process, various atomic coordinates were randomly assigned as the initial positions of the oxygen atoms [16]. The annealing process was restarted after finding a few oxygen

positions, until all oxygen positions were found to be reasonable. In this case, powder X-ray diffraction (PXRD) becomes a popular technique but with this technique, the possibility to determine an unknown structure dramatically decreases, because 3D reflections are compressed into 1D with an inevitable overlapping problem, especially when the unit cell is big. The situation will become worse when the PXRD is collected on a multi-phase sample, which is not uncommon in the preliminary stage of searching new materials, especially in the cases of hydrothermal (or solvothermal) syntheses of zeolitic or MOF materials'XRD data for the sample of $Bi_{0.5} Mn_{0.125} Mo_{0.5} O_{0.67}$ synthesized at its nominal composition is shown in Figure 1. All peaks could be indexed to a triclinic unit cell with *P-1*symmetry, analogous to the $Cu_{0.45} Mo_{1.25} O_9 V_{2.23}$ structure using CRYSFIRE PACKAGE[10]. In the diffraction pattern there is a slight anisotropic peak broadening moving to higher angles. This slight peak broadening could be caused by ordering within the cationic layers but relative disorder of the cations between layers. The sloping background observed in XRD at low angles out to ~30° 2θ is qualitatively indicative of stacking faults, a common feature of honeycomb oxides. In an ideal layered mixed-metal oxide, all the cationic planes are stacked along the c-axis by a unique translational stacking vector. However it has been shown that two other stacking vectors with very similar energy (1-2 meV) can occur in a structure, leading to so called "stacking faults". Stacking faults in the honeycomb oxides occur due to the relatively weak coupling between the layers In practice, the cationic layers are never perfectly stacked along the c-axis when a layered structure has the *P-1* space group, although higher temperature thermal treatment during synthesis can decrease the frequency of stacking faults[17].
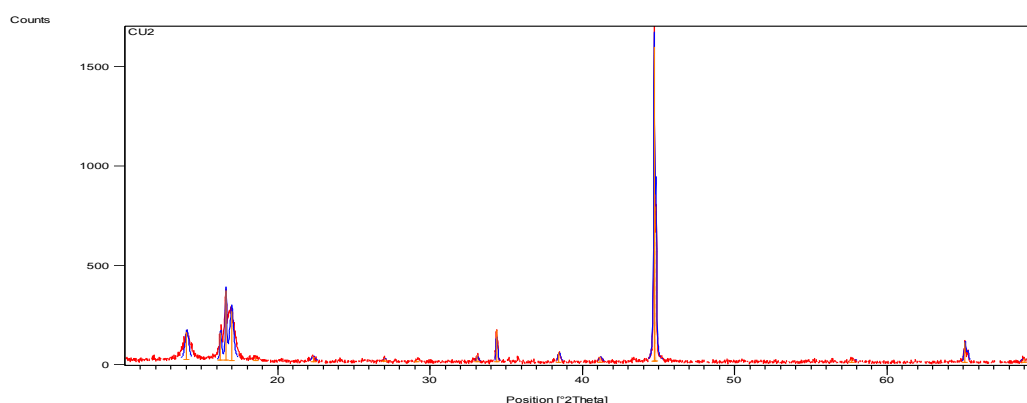

Figure1.XRD spectra of $Cu_{0.45} Mo_{1.25} O_9 V_{2.23}$
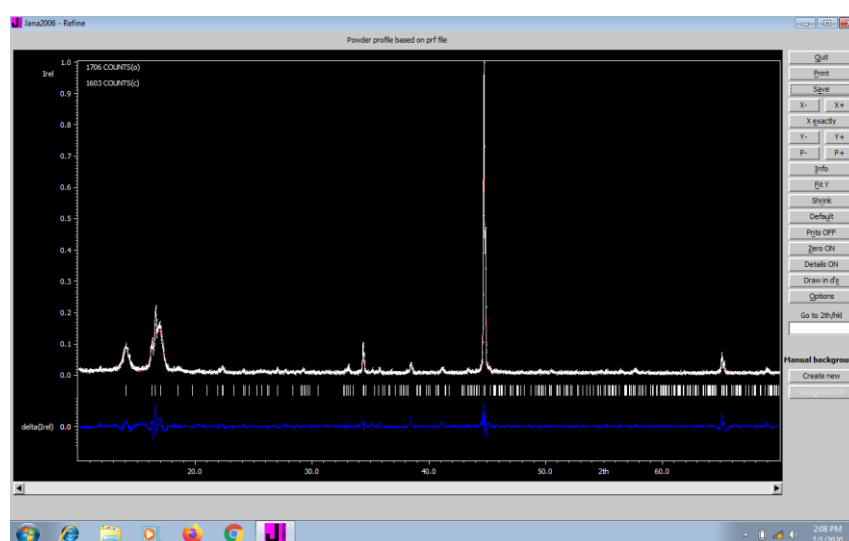

Figure2. Graphical representation of the result from Rietveld refinement with X-ray powder data. Vertical bars indicate positions of the Bragg reflections for $Cu_{0.45} Mo_{1.25} O_9 V_{2.23}$dots mark the observed intensities and the solid line gives the calculated intensity curve. The deviations

Table 2. Crystallographic data after Reitveld refinement

Creation method	Jana2006 Version : 25/10/2015

Phase data

Formula sum	$Cu_{0.45} Mo_{1.25} O_9 V_{2.23}$
Formula weight	406.1 g/mol
Crystal system	triclinic
Space-group	P -1 (2)
Cell parameters	a=4.8262 Å b=6.3208 Å c=10.4473 Å α=88.4808° β=85.0982° γ=85.0740°
Cell ratio	a/b=0.7635 b/c=0.6050 c/a=2.1647
Cell volume	316.30 $Å^3$
Z	2
Calc. density	4.26368 g/cm^3
Meas. density	2.43616g/cm^3
Pearson code	aP63
Formula type	N5O6P24Q28
Wyckoff sequence	i31f
Indexes	1≤ h≤,2,-2≤,k≤ 0,1≤,l≤,0

Fraction Coordinate

| Atom	Ox.	Wyck.	Site	S.O.F.	x/a	y/b	z/c	U [$Å^2$]
Mo1		1f	-1		1/2	0	1/2	0.0380
Mo2		2i	1		0.20055	-0.08780	0.41794	0.0380
Mo3		2i	1		0.39981	0.15415	0.02188	0.0380
Cu1		2i	1		0.22690	-0.36156	0.04203	0.0380
Cu2		2i	1		0.59173	0.49443	0.13513	0.0380
Cu3		2i	1		-0.16442	-0.08343	0.42080	0.0380
V1		2i	1		0.56065	-0.24925	0.41195	0.0380
V14		2i	1		0.72182	-0.28136	0.23249	0.0380
O1		2i	1		0.92498	-0.36264	-0.05578	0.0380
O2		2i	1		0.83375	-0.46660	0.62706	0.0380
O3		2i	1		0.56416	0.58811	0.03243	0.0380
O4		2i	1		0.29623	-0.12448	0.10132	0.0380
O12		2i	1		0.87764	-0.44414	0.45912	0.0380
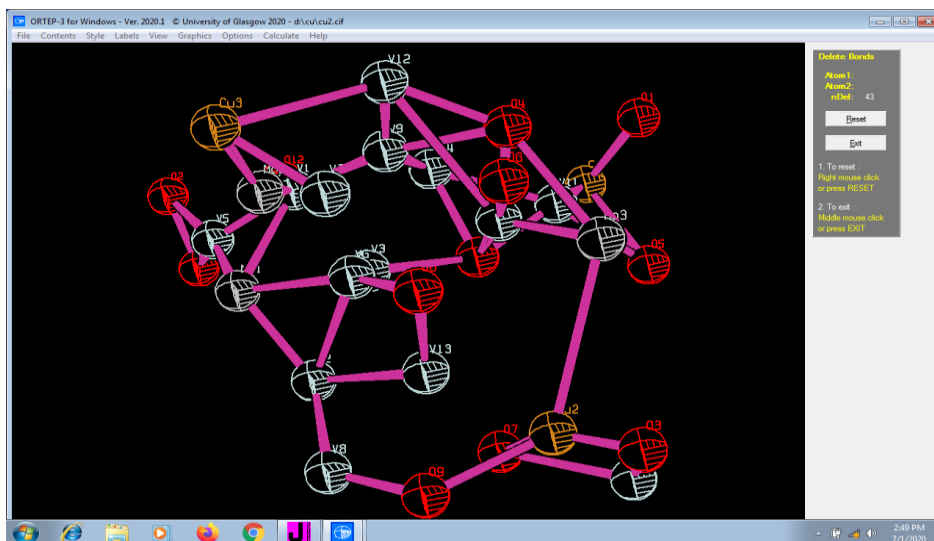
Figure3. Ortep diagram of $Cu_{0.45} Mo_{1.25} O_9 V_{2.23}$
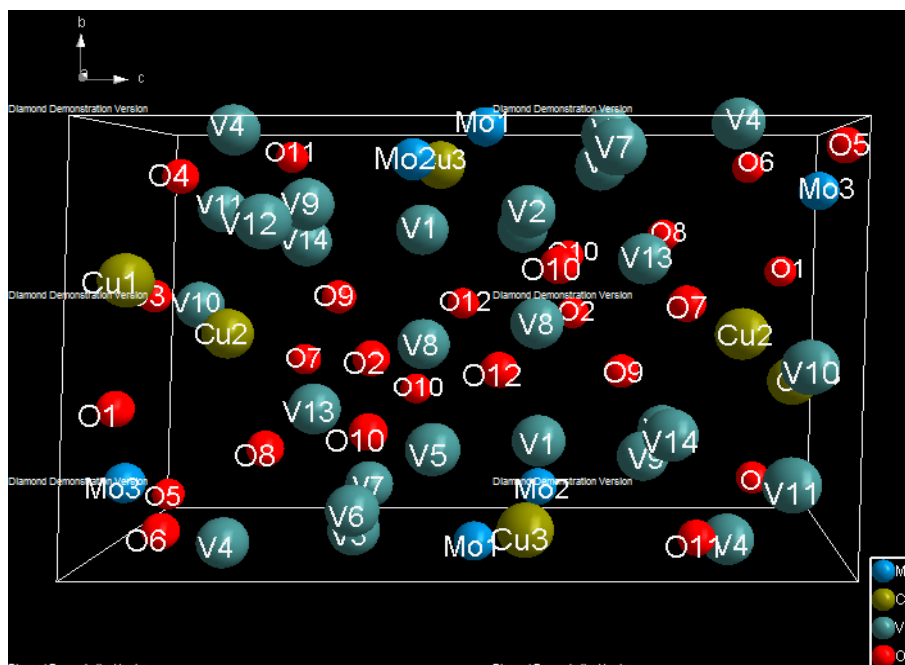
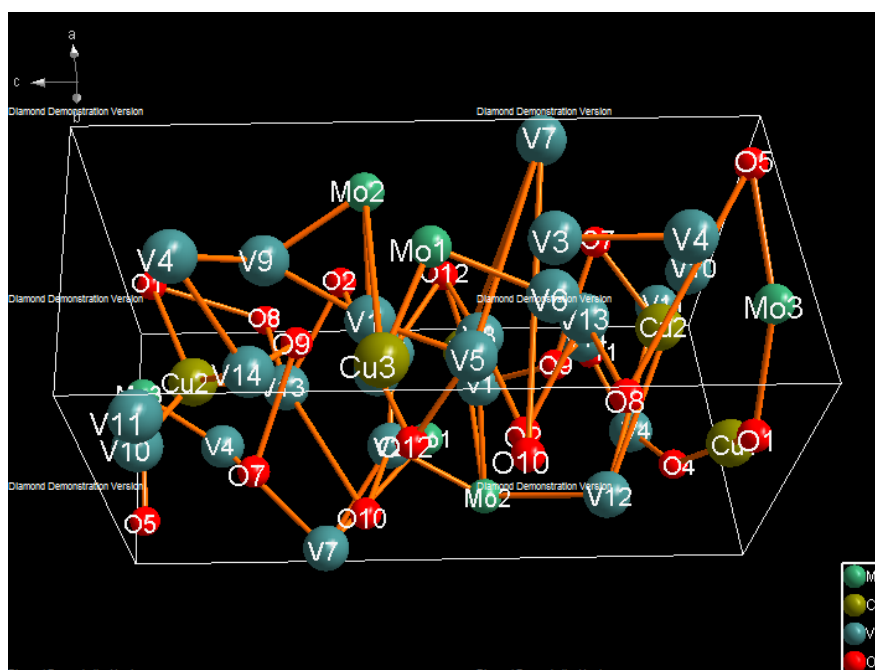**Figure 4.** Representation of the powellite-type crystal structures of $Cu_{0.45} Mo_{1.25} O_9 V_{2.23}$.atoms

Figure 5. Three dimension polyhedron structure of mixed valence of transition metal $Cu_{0.45} Mo_{1.25} O_9 V_{2.23}$

Table 2. Selected bond lengths

Atom1		Atom code	Atom2	Atom code2	Angle[0]
Mo1	V2	8656021	V2	8555011	180.000
	V2	8656021	Cu3	6655011	112.014
	V2	8656021	Cu3	6556021	67.986
	V2	8656021	V3	9555011	118.176
	V2	8656021	Mo2	2656021	116.929
	V2	8555011	Cu3	6655011	67.986
	V2	8555011	Cu3	6556021	112.014
	V2	8555011	Mo2	2656021	63.071
	V2	8555011	Mo2	2555011	116.929
	Cu3	6655011	Cu3	6556021	180.000
	Cu3	6655011	V3	9555011	61.804
	Cu3	6655011	Mo2	2656021	66.499
	Cu3	6556021	V6	12555011	92.809
	V1	7656021	Mo2	2555011	117.066
	V1	7656021	V6	12656021	79.174
V2	V6	12555011	Cu3	6555011	123.688
	V6	12555011	V12	18555011	89.640
	V6	12555011	V5	11656021	44.259
	Cu3	6555011	V1	7555011	149.165
	Cu3	6555011	V3	9555011	145.055
	Cu3	6555011	V12	18555011	74.621
Cu	Cu3	6556021	V12	18555011	163.132
	Cu3	6556021	V5	11656021	49.484
	V12	18555011	V5	11656021	126.754
	O6	26555011	V11	17655021	70.793
	O6	26555011	Mo3	3655021	100.739
	O6	26555011	O5	25755021	134.875
	O6	26555011	Cu1	4755021	155.737
	O6	26555011	V10	16665021	88.292
	V4	10555011	O3	23665021	136.751
V13	V6	12555011	O8	28555011	65.681

SEM(SCANNING ELECTRON MICROSCOPY)

Scanning electron microscopy (SEM) is giving morphological examination with direct visualization. The techniques based on electron microscopy offer several advantages in morphological and sizing analysis; however, they provide limited information about thesize distribution. For SEM characterization, nanoparticles solution should be first converted into a dry powder, which is then mounted on a sample holder followed by coating with a conductive metal, such as gold, using a sputter coater. The sample is then scanned with a focused fine beam of electrons. The surface characteristics of the sample are obtained from the secondary electrons emitted from the sample surface. The morphology of the transition metal mixed valece oxide nanoparticles is shown in Figure6. From the image, it is clear that the particles were highly agglomerated in nature. The SEM pictures clearly show randomly distributed grains with smaller size. From the SEM analyses, one can conclude the formation of nanoparticles spherical structure. Here it is grown in very high-density and possessing almost uniform spherical shapes. The image reveals that the average size of the particles is 70.32 nm.
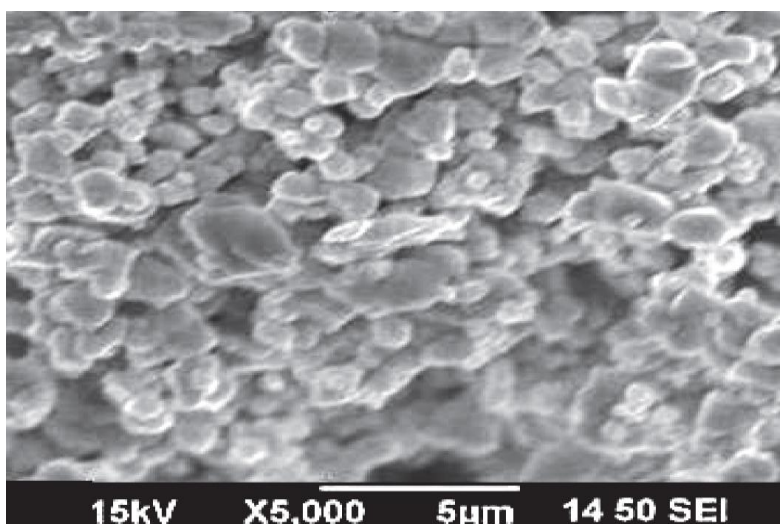

Figure.6: SEM image of nanoparticles of $Cu_{0.45} Mo_{1.25} O_9 V_{2.23}$

THE TRANSMISSION ELECTRON MICROSCOPE (TEM)

The transmission electron microscope utilized a high energy electron beam transmitted through a very thin sample to image and analyzes the microstructure of materials with atomic scale resolution. The electrons are focused with electromagnetic lenses and the image is observed on a fluorescent screen, or recorded on film or digital camera. The electrons are accelerated at several hundred kV, giving wavelengths much smaller than that of light: 200kV electrons have a wavelength of 0.025Å. Whereas, the resolution of the optical microscope is limited by the wavelength of light, that of the electron microscope is limited by aberrations inherent in electromagnetic lenses, to about 1–2 Å. Transmission electron microscope is used to characterize the microstructure of materials with very high spatial resolution. The transmission electron microscopic study was carried out to confirm the actual size of the particles, their growth pattern and the distribution of the crystallites. TEM image of the synthesized silver oxide nanoparticles is shown in Fig.3. As can be seen from the TEM image, the particles are nearly spherical shapes with well defined boundaries. It is evident from the micrographs that the average size of the particles as directly measured from the image is ~15 nm. This result is similar to that obtained from XRD analysis.
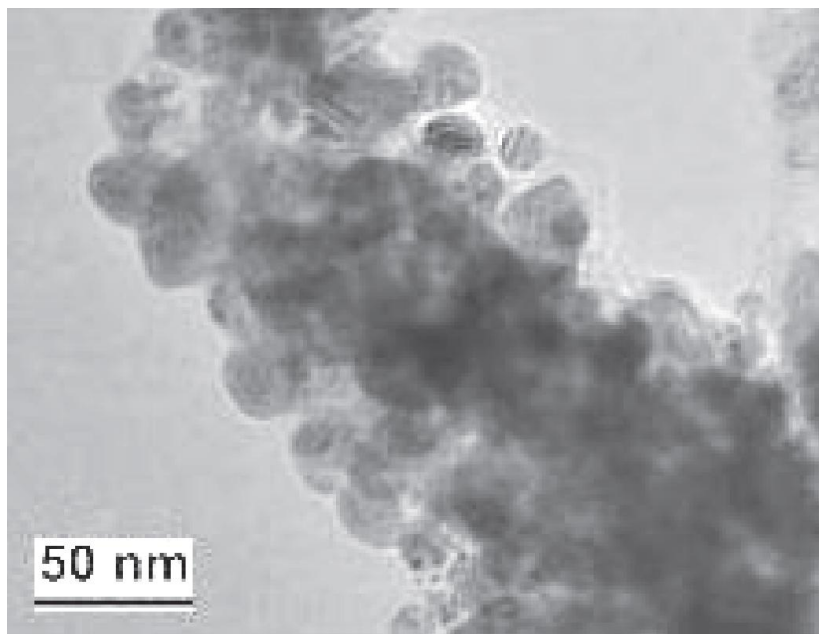
Figure7.TEM spectra of $Cu_{0.45} Mo_{1.25} O_9 V_{2.23}$

DIELECTRIC CONSTANT

The dielectric constant and the dielectric loss of the 10 mm in diameter pellet have been used for the determination of dielectric properties of silver oxide nanoparticles. The corresponding thickness of the pellet was 1.20 mm was studied at different temperature using a HIOKI 3532-50 LCR HITESTER in the frequency range of 50 Hz to 5 MHz. The results of the dielectric constant and dielectric loss as a function of frequency have been plotted in Figs. 8&9. It can be easily interpreted from the plots that the silver oxide nanoparticles show same trend, as having high values of dielectric constant and dielectric loss at low frequencies and decrease with the increase in frequency while reaching to a constant saturated value at high frequencies, depicting a frequency independent behavior. These defects activate interfacial polarizations at low frequencies. Due to this polarization, the dielectric constant is higher at low frequencies. The net polarization of silver oxide is owing to ionic, electronic, dipolar and space charge polarizations . The huge value of the dielectric constant is due to the fact that silver oxide acts as a nanodipole under electric fields [18]. The small-sized particles require a large number of particles per unit volume, important in an increase of the dipole moment per unit volume, and a high dielectric constant. The dielectric constant at low frequencies starts from high value and decreases with increase in temperature. As the temperature increases, the dielectric constant values start increasing. The high value of dielectric constant at low temperature credited to space charge polarization whereas at higher temperature and at low frequencies it possibly connected with defect related conduction processes . The variations of dielectric loss of silver oxide nanoparticles of with frequency and temperature are shown in Figure 11. It can be seen that dielectric loss decreases with increase of frequency and at higher frequencies the loss angle has almost the same value at all temperatures. In dielectric materials, generally dielectric losses take place due to absorption current. The orientation of molecules along the direction of the applied electric field in polar dielectrics requires a part of electric energy to overcome the forces of internal friction . One more part of electric energy is utilized for rotations of dipolar molecules and other kinds of molecular transfer from one position to another, which also involve energy losses. In nanophase materials, inhomogeneities similar to defects and space charge formation in the inter phase layers create an absorption current ensuing in a dielectric loss .
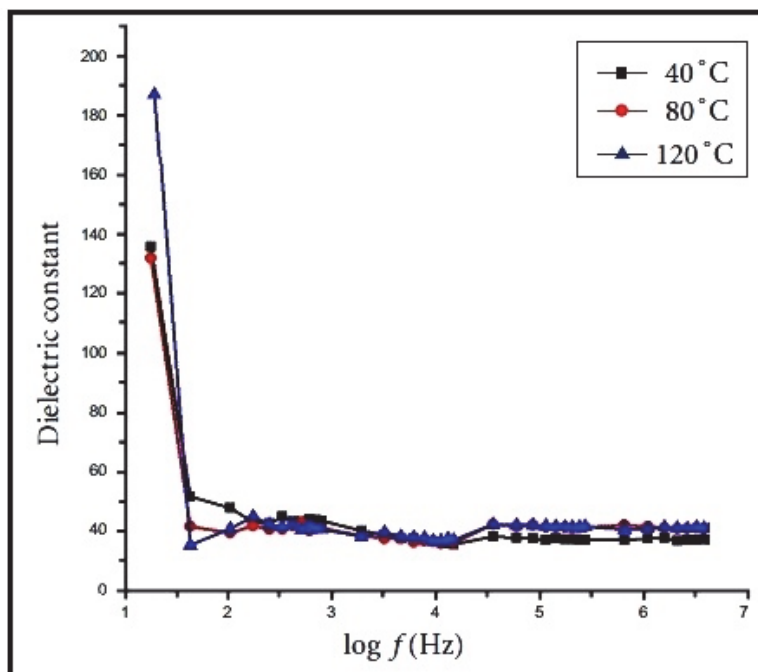
Figure 8: Dielectric constant as a function of log frequency

The titled metal oxide show nanopartice according to particle size which are placed in the heater and their response is taken at different temperatures. Temperature dependent dielectric constant and dielectric loss has been plotted in Figs. 8 and 9. It is also observed that as the temperature increases, the dielectric constant also increases to a considerable value as seen in Fig. 5. The same trend is observed behavior of dielectric properties with temperature is different over different temperature ranges i.e. at low and high temperature. It is evident from the Fig.6 and 7 that the dielectric constant and dielectric loss are low at a certain room temperature range and remain independent of temperature changes. In high temperature range the dielectric properties rise suddenly and reach a maximum value. The basic reason of the independency of dielectric constant in low temperature range is that impurities remain localized in this range and so conduction is not easy while at high temperature impurities are no more localized and hence conductivity of the material is increased. In case of ionic solids, electrons of the material also become free and contribute to conduction. This results in high polarization of the material; hence value of dielectric constant is increased with increase in temperature. At low and room temperature range, the effect of grain boundaries is dominant and that is why the dielectric properties have small magnitudes and are constant. As the temperature is increased, the role of grains becomes more and more effective and increases in the dielectric properties [20].
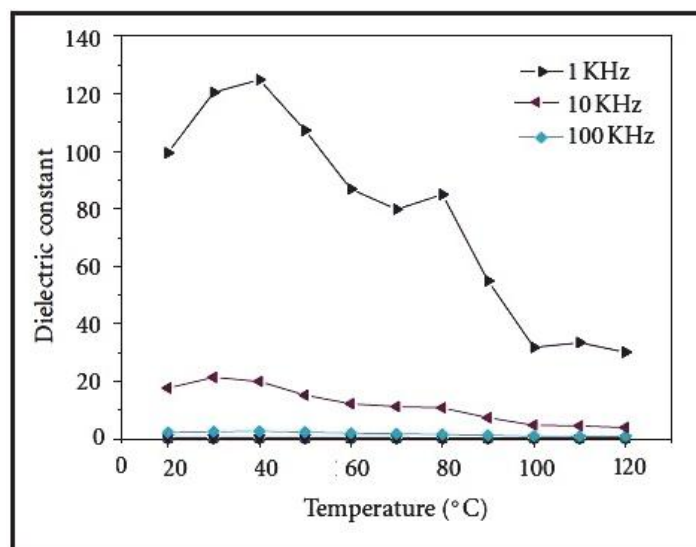

Figure9. Temperature dependent dielectric constant of $Cu_{0.45} Mo_{1.25} O_9 V_{2.23}$
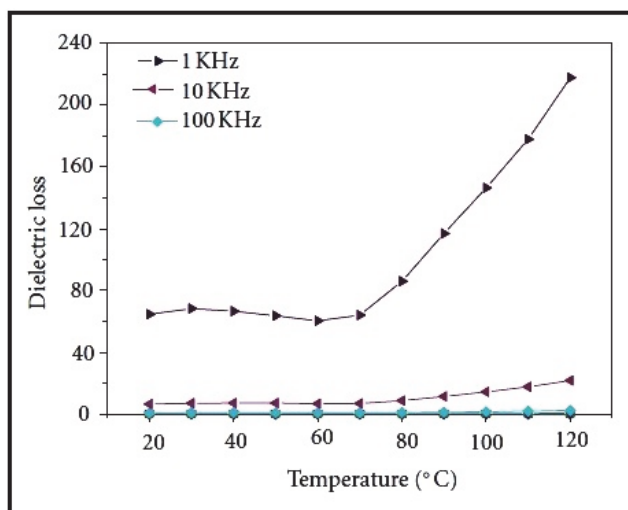
Figure10. Dielectric loss versus temperature as well given in Fig. 8. Nanoparticles

Due to the thermionic emission and tunnelling of charge carriers across the barrier, the conductivity increases with the temperature. Because of small size of the particles, the charge carriers reach the surface of the particles more and easily enabling the electron transfer by thermionic emission or tunneling to enhance the conductivity [16]. The a.c. conductivities strongly depend on the particle size, the concentration and heat treatment ofthe sample and the permeating of the electrolytes. Also, the frequency dependent data indicated that the enhancement was due to grains rather than grain boundary or surface conduction. The nature of frequency and temperature dependence of a.c. conductivity of the present samples, suggests an electronic hopping mechanism, exhibited by a large number of nanocrystalline materials. This hopping mechanism is compatible with the highly order and crystal structure of the grain boundary layers of nanophase materials, having high densities of localized levels. This polarization, which is out of phase with the applied electric field, is measured as a.c. conductivity
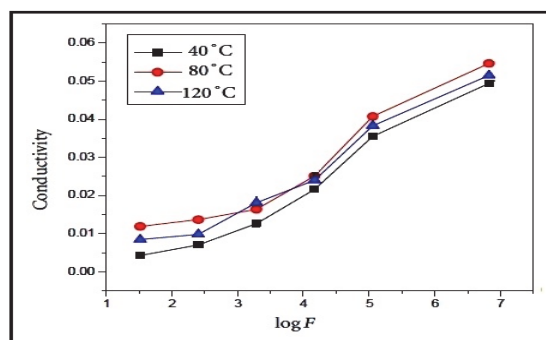

Figure11. Variation of conductivity with log f

IV. CONCLUSIONS

The titled transition metal mixed valence oxide have been successfully synthesized using stoichiometry chemical technique. X-ray diffraction analysis reveals that the crystallite size of the oxide \particles was found to be70.32 nm. Spherical shapes morphology of the prepared mixed valence metal oxide was observed in the SEM studies. The transmission electron microscopic analysis confirms the prepared $Cu_{0.45}$ $Mo_{1.25}$ O_9 $V_{2.23}$with the particle size of around70.32 nm. Absorption spectrum revealed that the extended absorption wavelength towards the visible-light region. The value of band gap energy obtained from UV absorption spectrum is 570 eV, which was also attributed to the formation of nanocrystalline particles. The variation of dielectric constant, dielectric loss with frequency and temperature for mixed valence metal oxide nanoparticles were analyzed. In addition, the plasma energy of the valence electron, Penn gap or average energy gap, the Fermi energy and electronic polarizability of the $Cu_{0.45}$ $Mo_{1.25}$ O_9 $V_{2.23}$ nanoparticles have been also determined. AC electrical conductivity was found to increase with an increase in the temperatures and frequency. The structure was demined by powder XRD using Rietveld refinement with help od Jana,Diamond and Ortep software package programe. This oxide will be shown as semi- conductivity character. The ac conductivity plot of the pelletized form of $Cu_{0.45}$ $Mo_{1.25}$ O_9 $V_{2.23}$nanoparticles is shown in Figure 11 .It is

observed from the results that the ac conductivity increases with the increase in temperature, which shows the semiconducting nature of the $Cu_{0.45}\,Mo_{1.25}\,O_9\,V_{2.23}$

REFERENCES

[1]. Parveen Rathi , Dharam Pal Singh , Parveen Surain , Synthesis, characterization, powder XRD and antimicrobial-antioxidant activity evaluation of trivalent transition metal macrocyclic complexes, C. R. Chimie 18 (2015) 430–437

[2]. Kai Li and Rik Van Deun, Novel Intense Emission-Tunable Li1.5La1.5WO6:Mn4+,Nd3+,Yb3+Material with Good Luminescence Thermal Stability for Potential Applications in c‑Si Solar Cells and Plant-Cultivation Far-Red-NIR LEDs, ACS Sustainable Chem. Eng. 2019, 7, 16284−16294

[3]. Peng, Q.; Cao, R.; Ye, Y.; Guo, S.; Hu, Z.; Chen, T.; Zheng, G. Photoluminescence properties of broadband deep-red-emitting Na2MgAl10O17:Mn4+ phosphor. J. Alloys Compd. 2017, 725, 139−144.

[4]. Liu, Y.; Gao, G.; Huang, L.; Zhu, Y.; Zhang, X.; Yu, J.; Richards, B. S.; Xuan, T.; Wang, Z.; Wang, J. Co-precipitation synthesis and photoluminescence properties of BaTiF6:Mn4+: an efficient red phosphor for warm white LEDs. J. Mater. Chem. C 2018, 6, 127−133.

[5]. Yu, Y.; Huang, Y.; Zhang, L.; Lin, Z.; Wang, G. Assessment of structure and spectral characteristics of new laser crystal Nd3+:KBaY- (MoO4)3. J. Alloys Compd. 2015, 651, 164−169.

[6]. Marciniak, Ł.; Bednarkiewicz, A.; Hreniak, D.; Strek, W. The influence of Nd3+ concentration and alkali ions on the sensitivity of non-contact temperature measurements in ALaP4O12:Nd3+ (A = Li, K, Na, Rb)nanocrystalline luminescent thermometers. J. Mater. Chem. C 2016, 4, 11284−11290.

[7]. Yang, Z.; Yang, J.; Qiu, J.; Song, Z. Comprehensive investigations of near infrared downshift and upconversion luminescence mechanisms in Yb3+ single-doped and Er3+,Yb3+ codoped SiO2 inverse opals. Phys. Chem. Chem. Phys. 2017, 19, 31997−32006.

[8]. Ye, S.; Zhou, J.; Wang, S.; Hu, R.; Wang, D.; Qiu, J. Broadband downshifting luminescence in Cr3+-Yb3+ codoped garnet for efficient photovoltaic generation. Opt. Express 2013, 21, 4167.

[9]. Reisfeld, R.; Lieblich-Soffer, N. Energy transfer from UO2 2+ to Sm3+ in phosphate glass. J. Solid State Chem. 1979, 28, 391−395.

[10]. Dexter, D. L.; Schulman, J. H. Theory of Concentration Quenching in Inorganic Phosphors. J. Chem. Phys. 1954, 22, 1063−1070.(49) Blasse, G.; Grabmaier, B. C. Luminescent Materials; Springer-Verlag: Berlin, Germany, 1994.

[11]. Wu, L.; Bai, Y.; Wu, L.; Yi, H.; Zhang, X.; Zhang, L.; Kong, Y.; Zhang, Y.; Xu, J. Analysis of the structure and abnormal photoluminescence of a red-emitting LiMgBO3:Mn2+ phosphor. Dalton Trans. 2018, 47, 13094−13105.

[12]. *Parashuram Mishra* Synthesis, crystal structure determination and ionic properties of novel BiCa0.5Mg0.5 O2.5 via X- ray powder diffraction data , Elixir Crystal Growth. 2041 32 (2011) 2041-2045.

[13]. T. Dan Vu, Firas Krichen, Maud Barre,† Sandrine Coste,† Alain Jouanneaux, Emmanuelle Suard,Andrew Fitch, and François Goutenoire Ab Initio Structure Determination of La34Mo8O75 Using Powder X-ray and Neutron Diffraction Data, DOI: 10.1021/acs.cgd.8b01552 Cryst. Growth Des. XXXX, XXX, XXX−XXX

[14]. Chambrier, M.-H.; Le Bail, A.; Giovannelli, F.; Redjaimia, A.;Florian, P.; Massiot, D.; Suard, E.; Goutenoire, F. La10W2O21: AnAnion-Deficient Fluorite-Related Superstructure with Oxide Ion Conduction. Inorg. Chem. 2014, 53, 147−159.

[15]. Lopez-Vergara, A.; Porras-Vazquez, J. M.; Infantes-Molina, A.; Canales -Vazquez, J.; Cabeza, A.; Losilla, E. R.; Marero-Lopez, D.Effect of Preparation Conditions on the Polymorphism and Transport Properties of La6−xMoO12−δ (0 ≤ x ≤ 0.8). Chem. Mater. 2017, 29,6966−6975.

[16]. Dmitri O. Charkin , Andrey S. Karpov , Sergey M. Kazakov , Igor V. Plokhikh ,Anastasiya I. Zadoya c, Alexey N. Kuznetsov a, Konstantin I. Maslakov a, Anton Yu Teterin d,Yury A. Teterin , Alexander N. Zaloga e, Oleg I. Siidra c, f Synthesis, crystal structure, spectroscopic properties, and thermal behavior of rare-earth oxide selenates, Ln2O2SeO4 (Ln ¼ La, Pr, Nd): The new perspectives of solid-state double-exchange synthesis, Journal of Solid State Chemistry 277 (2019) 163−168

[17]. Minfeng Lü, Marie Colmont, Houria Kabbour, Silviu Colis, and Olivier Mentré Revised Bi/M Layered Oxo-Sulfate (M = Co, Cu): A Structural andMagnetic Study,Inorganic Chemistry, dx.doi.org/10.1021/ic500877z | Inorg. Chem. 2014, 53, 6969−6978.

[18]. Jang-Yeon Hwang, Seung-Taek Myung, and Yang-Kook Sun Quaternary Transition Metal Oxide Layered Framework: O3-type Na[Ni0.32Fe0.13Co0.15Mn0.40]O2 Cathode Material for High-Performance Sodium-Ion Batteries, Journal of physical chemistry,DOI: 10.1021/acs.jpcc.7b12140 • Publication Date (Web): 10 Mar 2018